Combustion Theory and Modelling
Vol. 00, No. 00, Month 200x, 1–16

RESEARCH ARTICLE

Modelling flame turbulence interaction in RANS simulation of premixed turbulent combustion

Umair Ahmed[a*] and Robert Prosser[a+]

[a]*School of Mechanical, Aerospace and Civil Engineering, University of Manchester, M13 9PL, UK*

(*Received 00 Month 200x; final version received 00 Month 200x*)

Flame turbulence interaction ($\widetilde{\Delta}_c$) is an important term for modelling scalar dissipation ($\widetilde{\varepsilon}_c$) in premixed turbulent combustion. In order to obtain an accurate representation of the flame turbulence interaction phenomenon, an evolution equation for $\widetilde{\Delta}_c$ has recently been proposed. This equation gives a detailed insight into the flame turbulence interaction phenomenon and provides an alternative approach to model the important physics represented by $\widetilde{\Delta}_c$. In this paper the $\widetilde{\Delta}_c$ evolution equation is used to model a premixed propane-air flame stabilised in a turbulent mixing layer. The simulations are carried out in the context of a Reynolds Averaged Navier Stokes (RANS) framework and the results are compared with the experiments and also with the Large Eddy Simulation (LES). It is found that the modelling strategy involving the $\widetilde{\Delta}_c$ evolution equation gives good approximations for the mean velocities and flame locations in the mixing layer stabilised flame when compared with other modelling strategies.

Keywords: Flame turbulence interaction,Turbulence scalar interaction, Scalar dissipation, RANS modelling of strained premixed flames, Premixed turbulent combustion

1. Introduction

Obtaining an accurate and robust closure for the mean reaction rate in turbulent premixed reacting flows is challenging, and usually requires statistical methods. The total aerothermochemistry of the flow can be described entirely via a Probability Density Function (PDF) or, alternatively, statistical analysis may be limited to the fluid's composition. In the former approach, a multi dimensional PDF can in principle be calculated by using a PDF transport equation [1, 2]. This procedure circumvents a number of modelling assumptions and consequently produces quite general reaction rate models; its principal weakness stems from the modelling required to describe processes such as molecular diffusion. Another method known as the Conditional Moment Closure (CMC) [3] also exists. Recently this method has enjoyed some success for modelling premixed flames [4, 5], but more work is needed to make this approach robust for premixed combustion. One of the major problems associated with the CMC approach is the modelling of conditional scalar dissipation rate in premixed flames [6].

In many chemical reactions with high Damköhler number, the problem of closing the reaction rate is usually simplified under the thin flamelet assumption, according to which the reaction zone is assumed to be thin compared to the Kolmogorov length scale [7, 8]. In

*Corresponding author. Email: umair.ahmed@manchester.ac.uk

+ Email: robert.prosser@manchester.ac.uk

ISSN: 1364-7830 print/ISSN 1741-3559 online

DOI: 10.1080/13647830.YYYY.xxxxxx
http://www.tandfonline.com

the thin flamelet approach the flame is assumed to consist of a very thin sheet separating products from reactants, and whose local structure is that of a laminar flame [7, 9]. All of the effects of the combustion chemistry and related transport effects are limited to the interface, and thus it becomes possible to approximate the thermochemistry via a single Presumed Probability Density Function (PPDF) of a *reaction progress variable* (denoted by c and usually defined as a normalised scalar mass fraction), comprising a double delta function representing the unburnt and burnt mixtures [10, 11]. This approximation leads to simple and elegant closures for a number of turbulence related terms. Using the flamelet assumption and PPDF framework, several approaches are available in the literature to close the reaction rate and include; the G-equation [12]; laminar flamelets [13, 14]; flame surface density models [15, 16] and scalar dissipation rate based approaches [17]. Two approaches are widely used under the thin flamelet assumption, namely the flame surface density (Σ) approach and the scalar dissipation $(\widetilde{\varepsilon}_c)$ approach. In premixed combustion, the scalar dissipation rate and the flame surface density are algebraically related to each other [18]. The scalar dissipation in premixed combustion represents the average rate at which hot products and cold reactants mix on the flame surface to sustain combustion [19], while the flame surface density represents the flame surface area per unit volume [20]. In this study both of these approaches are used.

The aim of this study is to asses the performance of the newly proposed flame turbulence interaction transport equation of Ahmed et al [21] and compare it with different modelling strategies for closing flame turbulence interaction including the algebraic models proposed by Kolla et al [22], Vervisch et al [23] and the flame surface density based approach. A rearward facing step of Pitz and Daily [24, 25] is chosen as a test configuration for this study.

The paper is organised as follows; in the next section we briefly describe the mathematical background for combustion models. The test case being studied and the numerical procedure used for the calculations is described in section 3, followed by the discussion of the results obtained from the simulations. Finally the conclusions are summarised in the last section.

2. Mathematical background for reacting flow calculations

In this paper a transport equation for the Favre averaged progress variable $\widetilde{c}$ is solved along with the variance of the progress variable $\widetilde{c''^2}$, and the relevant fluid dynamic equations. The progress variable can be described in terms of scalar mass fraction or temperature, here it is defined in terms of fuel mass fraction (Y_F) as :

$$c \equiv \frac{Y_F - Y_{FR}}{Y_{FP} - Y_{FR}}, \tag{1}$$

where the subscripts R and P denote the reactant and product side of the flame respectively. A transport equation for the Favre averaged progress variable can be written as :

$$\frac{\partial \overline{\rho}\widetilde{c}}{\partial t} + \frac{\partial \overline{\rho}\widetilde{u}_i\widetilde{c}}{\partial x_i} = -\frac{\partial \overline{\rho u_i'' c''}}{\partial x_i} + \overline{\dot{\omega}}_c, \tag{2}$$

where closures for the mean reaction rate $(\overline{\dot{\omega}}_c)$ and the turbulent transport $(\overline{\rho u_i'' c''})$ are needed (double primes denote the Favre fluctuations). The transport equation for the vari-

ance of the progress variable is :

$$\frac{\partial \overline{\rho}\widetilde{c''^2}}{\partial t}+\frac{\partial \overline{\rho}\widetilde{u}_i\widetilde{c''^2}}{\partial x_i}=-\frac{\partial \overline{\rho u_i'' c''^2}}{\partial x_i}-2\overline{\rho}\widetilde{\varepsilon}_c-2\overline{\rho u_i'' c''}\frac{\partial \widetilde{c}}{\partial x_i}+2\overline{c''\dot{\omega}_c}. \tag{3}$$

In this study turbulent transport in the above transport equations is modelled by a gradient diffusion model, despite the fact that countergradient diffusion may occur in premixed flames of practical interest [26]. The reasoning behind the model choice is twofold: (1) the uncertainty associated with closures embodying countergradient effects introduce additional uncertainty into the calculations, and typically have only small additional benefit for lower levels of turbulence intensities [27, 28], and; (2) the behaviour of the flame turbulence interaction model and its effect on the reaction rate closure (which is the main focus of the current work) can be studied by using the gradient diffusion approach [22, 29]. As mentioned before the source term in eq. (1) can be closed in terms of $\widetilde{\varepsilon}_c$ and Σ. In the $\widetilde{\varepsilon}_c$ approach $\overline{\dot{\omega}}_c$ is closed as [17]:

$$\overline{\dot{\omega}_c} \backsimeq \frac{2}{2C_m-1}\overline{\rho}\widetilde{\varepsilon}_c, \tag{4}$$

where $\widetilde{\varepsilon}_c$ is the scalar dissipation $\left(\overline{\rho}\widetilde{\varepsilon}_c=\overline{\rho\alpha\left(\nabla c''\nabla c''\right)}\right)$, α represents the diffusivity of the progress variable and C_m is a model constant with a value of 0.7 in hydrocarbon flames. While in the Σ approach the $\overline{\dot{\omega}}_c$ is closed as [17]:

$$\overline{\dot{\omega}_c} \backsimeq \rho_R u_L^0 \Sigma. \tag{5}$$

The source term in eq. (3) is closed as [17]:

$$\overline{\dot{\omega}_c'' c''}=(C_m-\widetilde{c})\overline{\dot{\omega}_c}. \tag{6}$$

In the above equations the problem of modelling the reaction rate has been reduced to that of modelling either the scalar dissipation rate or the flame surface density. There are several approaches available in the literature to close $\widetilde{\varepsilon}_c$ and Σ; some of these approaches are discussed in the following subsections.

2.1 *Scalar dissipation rate transport equation*

A transport equation for $\widetilde{\varepsilon}_c$ has been proposed by Swaminathan and Bray, which under joint assumptions of high Reynolds (Re) and Damköhler (Da) numbers can be written as [30]:

$$\overline{\rho}\frac{D\widetilde{\varepsilon}_c}{Dt}=T_{11}+T_2+T_{32}+T_4-D_2. \tag{7}$$

Each of the terms on the right hand side of eq. (7) represent a particular physical process. Term T_{11}represents the turbulent transport of $\widetilde{\varepsilon}_c$. T_2 represents the effects of dilatation due to density gradients caused by heat release. T_{32} represents the effects of flame turbulence interaction. T_4 represents the effects of reaction rate and D_2 represents the molecular diffusion/dissipation effects in $\widetilde{\varepsilon}_c$ transport equation. The exact expressions for the terms on the right hand side of eq. (7) are given in appendix-A.

Term T_{11} in eq. (7) is closed by using a gradient diffusion model. Term T_2 representing dilatation is closed as [22]:

$$T_2 \approx 2K_c^* \overline{\rho} \widetilde{\varepsilon}_c \left(\frac{u_L^0}{\delta_L^0} \right), \tag{8}$$

where $K_c^* \approx 0.85\tau$ (τ is the heat release parameter $\tau = (T_P - T_R)/T_R$) for hydrocarbon flames, and u_L^0 and δ_L^0 represent the unstrained laminar flame speed and the thermal flame thickness respectively. The combination $(T_4 - D_2)$ containing the reaction rate and dissipation effects is closed as [31]:

$$T_4 - D_2 \approx -\beta^{'} \overline{\rho} \frac{\widetilde{\varepsilon}_c^2}{\widetilde{c^{''2}}}, \tag{9}$$

where $\beta^{'} \approx 6.7$ and $\widetilde{c^{''2}}$ is closed by using the variance transport equation in eq. (3). It has been found in earlier studies that terms T_2 and $T_4 - D_2$ have robust closures and perform well over a range of different Reynolds and Karlovitz numbers [22, 31–33], while term T_{32} poses a problem at higher Reynolds and Karlovitz numbers as the existing closures either under predict or over predict the value for different Reynolds numbers [33, 34]. Hence a robust closure for T_{32} is needed for accurate modelling of scalar dissipation. Here T_{32} is defined as :

$$T_{32} = -2\overline{\rho} \widetilde{\Delta}_c, \tag{10}$$

where $\widetilde{\Delta}_c$ is the flame turbulence interaction. In this paper we test two closure strategies for $\widetilde{\Delta}_c$, one approach is to close $\widetilde{\Delta}_c$ algebraically and the other approach is to use a modelled transport equation. Both of these modelling strategies are briefly discussed in the next subsections.

2.1.1 Algebraic model for flame turbulence interaction

An algebraic model for flame turbulence interaction has been proposed by Kolla et al [22]. The model is constructed on the assumption that the flame turbulence interaction is controlled by the competition between turbulent and chemical time scales, and is written as [22]:

$$\widetilde{\Delta}_c \approx -\frac{1}{2} \left[C_3 - \tau C_4 Da_L^* \right] \left(\frac{\widetilde{\varepsilon}}{\widetilde{k}} \right) \widetilde{\varepsilon}_c. \tag{11}$$

C_3 and C_4 in eq. (11) are scaling factors for the model and are defined as [14]:

$$C_3 = 1.5 \left(\frac{\sqrt{Ka_L}}{(1+\sqrt{Ka_L})} \right) \quad \text{and} \quad C_4 = \frac{1.1}{(1+Ka_L)^{0.4}}, \tag{12}$$

where Ka_L is the local Karlovitz number and is calculated as :

$$Ka_L = (u^{'}/u_L^0)^{3/2} (\delta_L/l_t)^{1/2}. \tag{13}$$

In eq. (13) δ_L is the flame diffusion thickness $\delta_L = \delta_L^0/(2(1+\tau)^{0.7})$ [35]. Da_L^* in eq. (11) represents the effects of local Damkhöler number based on the flame thermal thickness

[22, 32]:

$$Da_L^* = \frac{u_L^0/\delta_L^0}{\widetilde{\varepsilon}/\widetilde{k}}. \tag{14}$$

$u^{'}$ and l_t in eq. (11) are defined as :

$$u^{'} = \sqrt{\frac{2\widetilde{k}}{3}} \text{ and } l_t = \frac{u^{'3}}{\widetilde{\varepsilon}}, \tag{15}$$

where $\widetilde{k}$ and $\widetilde{\varepsilon}$ are calculated from the turbulence model being used in the simulation. The model in eq. (11) is referred to as FTI algebraic model in the following sections.

2.1.2 Flame turbulence interaction transport equation

A transport equation for flame turbulence interaction has recently been proposed by Ahmed et al [21]. This equation provides insight into the physical mechanisms which control flame turbulence interaction. In the same sense as scalar dissipation transport equation (eq. (7)) a transport equation for $\widetilde{\Delta}_c$ can be derived; the transport equation under joint assumptions of high *Re* and *Da* numbers can be written as [21]:

$$\overline{\rho}\frac{D\widetilde{\Delta}_c}{Dt} = -\frac{\partial\overline{\rho u_i^{''}\Delta_c^{''}}}{\partial x_j} + D_f + F_1 + F_D + F_{Ts}. \tag{16}$$

In eq. (16), D_f represents the diffusion/dissipation process due to molecular effects. F_1 represents the influence of the reaction rate and the pressure Hessian on $\widetilde{\Delta}_c$. F_D represents the influence of dilatation due to heat release and F_{TS} represents the influence of turbulent straining. Note that in the $\widetilde{\Delta}_c$ transport equation there is a competition between turbulent and chemical time scales along with a competition between diffusion/dissipation, reaction rate and pressure Hessian terms. The exact expressions for the terms on the right hand side of eq. (16) are given in appendix-A.

Turbulent transport of $\widetilde{\Delta}_c$ is closed by using the gradient diffusion hypothesis. The combined effects of reaction rate, diffusion/dissipation and pressure Hessian $\left(D_f + F_1\right)$ are closed as [21]:

$$D_f + F_1 \approx C_a\overline{\rho}\frac{\widetilde{\Delta}_c^2}{\widetilde{\varepsilon}_c}. \tag{17}$$

The turbulent straining effects represented by term F_{TS} are closed as [21]:

$$F_{TS} \approx C_b\overline{\rho}\frac{\widetilde{\varepsilon}}{\widetilde{k}}\widetilde{\Delta}_c. \tag{18}$$

The effects of dilatation represented by term F_D are closed as [21]:

$$F_D \approx C_c Da_L\overline{\rho}\widetilde{\Delta}_c\tau\frac{u_L^0}{\delta_L}. \tag{19}$$

where u_L^0 is the unstreached laminar flame speed, δ_L is the flame diffusion thickness. In the above equations C_a, C_b and C_c are scaling factors for the models and are listed in table

1. These scaling factors have been developed and validated in a previous DNS study by Ahmed et al [21]. The quantities Re_{l_t}, Ka_L and Da_L in table (1) and eq. (17) - eq. (19) are the turbulent Reynolds number, local Karlovitz number and local Damköhler number based on flame diffusion thickness respectively. Ka_L is calculated by using eq. (13), while Re_{l_t} and Da_L are calculated as :

$$Re_{l_t} = \frac{u^{'} l_t}{\nu_R}, \quad Da_L = \frac{u_L^0/\delta_L}{\widetilde{\varepsilon}/\widetilde{k}}. \tag{20}$$

ν_R in eq. (20) is the kinematic viscosity of the reacting mixture. $u^{'}$ and l_t in the above equations are calculated by using eq. (15). This model is referred to as FTI transport model in the following sections.

2.2 *Algebraic scalar dissipation models*

Algebraic models for scalar dissipation can be obtained from the leading order terms of the $\widetilde{\varepsilon}_c$ transport equation [30]. Kolla et al [22] have proposed a model by using the closures of the leading order terms in the scalar dissipation transport equation as:

$$\widetilde{\varepsilon}_c \approx \left(2K_c^* \frac{u_L^0}{\delta_L^0} + C_3 \frac{\widetilde{\varepsilon}}{\widetilde{k}} - \tau C_4 Da_L^* \frac{\widetilde{\varepsilon}}{\widetilde{k}} \right) \frac{\widetilde{c^{''2}}}{\beta^{'}}, \tag{21}$$

where the model constants are the same as defined in section 2.1. $\widetilde{c^{''2}}$ in eq. (21) is closed by using the variance transport equation in eq. (3). This model is referred to as algebraic SDR 1 model in the following sections.

The scalar dissipation rate can also be closed algebraically in terms of flame surface density as proposed by Vervisch et al [23]:

$$\widetilde{\varepsilon}_c \approx \frac{(1+\tau\widetilde{c})}{2} (2C_m - 1)\, u_L^0 \Sigma \left(\frac{\widetilde{c^{''2}}}{\widetilde{c}(1-\widetilde{c})} \right), \tag{22}$$

where Σ is the flame surface density and embodies the combined effects of flame turbulence interaction, and the remaining terms represent the combined effects of dilatation and reaction rate. $\widetilde{c^{''2}}$ in eq. (22) is closed by using the variance transport equation in eq. (3). The closure for flame surface density is explained in the next sub section. This model is referred to as algebraic SDR 2 model in the following sections.

2.3 *Closure for flame surface density*

In order to close the reaction rate via eq. (5) and scalar dissipation via eq. (22) a closure for flame surface density is needed. In this paper the flame surface density is closed by the most common form of the closed transport equation for Σ as [29, 35]:

$$\frac{\partial \Sigma}{\partial t} + \frac{\partial \widetilde{u}_i \Sigma}{\partial x_i} = \frac{\partial}{\partial x_i} \left(\frac{\nu_t}{\sigma_\Sigma} \frac{\partial \Sigma}{\partial x_i} \right) + \underbrace{\alpha_0 \frac{\widetilde{\varepsilon}}{\widetilde{k}} \Sigma}_{a} - \underbrace{\beta_0 \langle s_c \rangle_s \frac{\Sigma^2}{1-\widetilde{c}}}_{b}, \tag{23}$$

where α_0 and β_0 are model constants and generally take values of 1.7 and 1.0 respectively [36]. Terms a and b in eq. (23) represent the effects of tangential straining and flame

curvature, respectively, and $\langle s_c \rangle_s \approx u_L^0$ (to first order) represents the consumption speed [35]. Term b in eq. (23) is introduced to mitigate the infinite flame growth driven by the generally positive tangential strain rate contribution [35]. The model using eq. (5) and eq. (23) is referred to as FSD model in the following sections.

3. Test configuration and numerical procedure

The experiments performed by Pitz and Daly [24, 25] are considered in this paper. The case under consideration is a propane-air premixed flame with an equivalence ratio (ϕ) of 0.57. A sketch of the experimental configuration can be seen in figure 1. The experiment consists of a rectangular premixing region followed by a smooth contraction to one-half of its height (not shown in figure 1). There follows a step expansion into the combustion region and a quenching water spray filled converging exit region. Note that in the simulations, the smooth contraction at the inlet is omitted, as there is no data available for it and no attempt is made to represent the effects of the spray at the exit. However the converging exit region is simulated in order to move the outlet boundary condition sufficiently far from the recirculation region. The flame is stabilised in a turbulent-free shear layer formed at the backward facing step. The mean inlet values for the bulk velocity, pressure and temperature are given in table 2. The Reynolds number based on bulk velocity and step height is $Re = 22100$. The experimental measurements were performed using Laser Doppler Velocitmetry (LDV) gas analysis and schileren imaging techniques with a measurement error of approximately $0.1\% - 0.4\%$ for mean velocities [24]. Further details of the experiment and measuring techniques used can be found in [24, 25]. This test case has been previously studied by Weller et al [37] (using flame wrinkling model) and Fureby [38] (using the newly proposed homogenisation based method) via Large Eddy Simulation (LES) and by Tangermann et al [39] (using a modified flame surface density model) via both Large Eddy Simulation (LES) and Reynolds Averaged Navier Stokes (RANS) approaches. This case represents a dump combustor configuration in gas turbine engines.

The calculations for this work have been performed using the unstructured finite volume code, *Code_Saturne* [40] (see: www.code-saturne.org). This code has previously been used by Jarrin et al [41] for isothermal flow simulations and by Dong et al [42] for reacting flow calculations. The code solves the Navier Stokes equations for Newtonian incompressible flows with a fractional step method based on a prediction-correction algorithm for pressure/velocity coupling (SIMPLEC) and a Rhie and Chow interpolation to avoid pressure oscillations. The code uses second order central differencing scheme for spatial gradients; the time integration is done by an Euler explicit scheme. The time steps during the simulations are set to achieve a maximum CFL number of 0.4 for stability of the solution. The simulations are run until a statistically steady flow (all the statistics are invariant under a shift in time) is achieved. Dirichlet conditions are used at the inlet for all variables except pressure, for which a zero Neumann condition is applied. At the outlet all the variables are treated with a zero Neumann condition except pressure for which a Dirichlet condition is used. A no-slip condition is applied to the velocity at the walls along with appropriate wall treatment, while all the scalars are treated with zero Neumann conditions. Symmetry conditions are used in the transverse direction. Similar boundary conditions have been used in the earlier study of Weller et al [37] for the same rearward facing step.

4. Results and discussion

4.1 *Isothermal flow calculation*

In order to establish the accuracy of the turbulence models in a cold flow configuration, isothermal flow calculations are performed. Initially the simulations are performed with the standard $k-\varepsilon$ model proposed by Jones and Launder [43] and also with the $k-\omega$ SST model proposed by Menter [44]. The details of the turbulence models used in this study are given in appendix-B. The computational grids used for the $k-\varepsilon$ and $k-\omega$ SST models are shown in figures 2a and 2b respectively. Note that the $k-\varepsilon$ model uses a standard wall function near the walls and requires a y^+ of 30 at the wall, while the $k-\omega$ SST model does not require a wall function, and a y^+ of 1 at the wall is needed. Mesh sensitivity studies have been carried out and the two meshes shown in figure 2 give mesh independent results. The mesh for $k-\varepsilon$ model requires 20000 cells while the mesh for $k-\omega$ SST model is 25000 cells. Velocity and turbulence intensity profiles for the simulations are taken from the experiment of Pitz and Daily [24, 25] and are shown in figure 3. The integral length scale at the inlet is specified as $l_t \approx 0.0254m$.

Both the $k-\varepsilon$ and $k-\omega$ SST models predict similar flow velocities in this case as shown in figure 4. There is a slight disagreement of the velocity in the recirculation region, causing a small discrepancy in the predicted flow velocity further downstream of the backward facing step. This behaviour of the turbulence models is expected, as it is well known that these models tend to produce erroneous results for the prediction of separation regions [45, 46]. Figure 5 shows the velocity contours for both of the turbulence models used. It can be seen in figure 5 that the size of the recirculation bubble predicted by the $k-\varepsilon$ and the $k-\omega$ SST models is $x_r/h \approx 6.7$ and $x_r/h \approx 7.4$ respectively. The size of the recirculation bubble predicted by both models is slightly wrong when compared with the experimental value of $x_r/h \approx 7.0$. These results are consistent with those of Furbo [47] for this geometry and Klein et al [48] for a generic backward facing step. In these earlier studies it has been shown that the two equation model with wall functions tend to perform well when compared with other turbulence models (including second moment closures). Here the performance of the standard $k-\varepsilon$ model with wall functions is considered to be satisfactory. Hence the standard $k-\varepsilon$ model is used for the reacting flow simulations, due to the smaller mesh size and lower computational costs associated with it.

4.2 *Reacting flow calculation*

In order to compare the performance of the combustion models presented in section 2, reacting flow simulations of the mixing layer have been performed. In the reacting case, the incoming fluid contains cold premixed reactants, which mix with the hot products in the shear layer formed behind the backward facing step and subsequently burn. The shear layer effectively anchors the flame to the backward facing step. The unstrained laminar flame speed (u_L^0) used for the propane air mixture at $\phi = 0.57$ and $T_0 = 293K$ is $0.09m/s$ [49, 50] and the kinematic viscosity of the reacting mixture (ν_R) is specified as $2.183 \times 10^{-5} m^2/s$. The flame thermal thickness in the simulations is calculated as [51]:

$$\delta_L^0 = \frac{\nu_R}{u_L^0} \times 2(1+\tau)^{0.7}.$$

Due to the presence of the walls a special treatment for the SDR1, SDR2 and FSD models is needed, as these models predict reaction in the boundary layer formed at the top wall. In order to rectify this problem we use the quenching model proposed by Catlin and Lindstedt [52]. This model suppresses the reaction rate if the progress variable falls below

a quenching value $\widetilde{c}_q$, which in case of adiabatic conditions corresponds to a quenching temperature $T_q = \widetilde{c}_q (T_P - T_R) + T_R$. In the calculations the reaction is suppressed if the temperature falls below T_q. Several values for T_q have been tested and it is found that a value of $300K$ results in no reaction in the boundary layer at the top wall. Hence a value of $300K$ is used for T_q in the SDR1, SDR2 and FSD models. A similar strategy for suppressing the reaction rate has been adopted by Tangermann et al [39] in their study of the same backward facing step. Note that the models based on $\widetilde{\varepsilon}_c$ transport equation do not require such treatments as they account for flow history effects on the evolution of $\widetilde{\varepsilon}_c$ via the $\widetilde{\varepsilon}_c$ transport equation. Thus accounting for fluid mechanics effects on the reaction rate, and do not predict high reaction rate near the walls.

In the reacting case the length of the recirculation zone is shorter than in the cold flow case, as seen in figure 6. The length of the recirculation zone predicted by the FSD, SDR1, SDR2, FTI (algebraic) and FTI (transport equation) models is $x_r/h \approx 4.1$, $x_r/h \approx 4.4$, $x_r/h \approx 4.2$, $x_r/h \approx 4.6$ and $x_r/h \approx 4.5$ respectively. The recirculation length predicted by the SDR1, FTI (algebraic) and FTI (transport equation) models is in good agreement with the experimental value of $x_r/h \approx 4.5$.

It can be seen from figure 7 that the SDR1, SDR2 and FSD models predict higher velocities near the recirculation region at $x/h = 1$ and $x/h = 3$ when compared with both of the FTI models, LES and experimental data. This is due to the higher reaction rate predicted by the models in these regions as shown in figures 8 and 9. In case of the FSD and SDR2 models the higher reaction rate prediction is due to the dependence of the Σ transport equation on $\widetilde{k}$ and $\widetilde{\varepsilon}$, which are used to model the turbulent time scales. Hence $\overline{\dot{\omega}}_c \to \infty$ as $\widetilde{k} \to 0$ at the wall. Similarly in case of the SDR1 model the ratio $\widetilde{\varepsilon}/\widetilde{k}$ is high near the wall, thus leading to high reaction rates in those regions. As mentioned before the FTI (algebraic) and the FTI (transport equation) models do not have these problems due to the inclusion of flow history effects through the $\widetilde{\varepsilon}_c$ transport equation. Thus leading to very small contributions from terms containing $\widetilde{\varepsilon}/\widetilde{k}$ in the near wall regions for $\widetilde{\varepsilon}_c$ and $\widetilde{\Delta}_c$ transport equations.

Both FTI models under predict the recirculation velocity at $x/h = 1$ in figure 7. This behaviour is expected as the $k-\varepsilon$ model tends to under predict the velocity in recirculation regions due to its poor performance in regions of rapid straining and strong shear [46, 48]. The performance of SDR1, SDR2 and FSD models improves at $x/h = 5$, although there is a small discrepancy between $y/h = -0.5$ and $y/h = 0$ as shown in figure 7c, while the FTI algebraic model tends to under predict the velocity at $x/h = 5$ between $y/h = 0$ and $y/h = -1$. Further downstream the SDR1 and FSD models predict higher velocities while the SDR2 and FTI (algebraic) models tend to under predict the velocity at $x/h = 7$ between $y/h = -1$ and $y/h = 0$ as shown in figure 7d. The variation in the prediction of mean velocities by different models is due to a difference in the prediction of the reaction rates at the respective locations as shown in figure 8.

Generally the velocity profiles predicted by the FTI (transport equation) model are in good agreement with the experimental data, and the predicted velocity profiles improve as the distance from the stabilisation region increases. FTI transport equation yields better results away from the rearward facing step when compared with other models, as it explicitly includes the strain rate and its flow history effects through the inclusion of the source term (pressure Hessian in term F_1 of eq (16)) for the strain rate transport equation.

Figures 8 and 9 show a large variation in the prediction of reaction rates from different models at several locations downstream of the rearward facing step. These variations can be explained by differences in the underlying assumptions for different models. As mentioned earlier the high reaction rate predictions near the walls (figure 8a) from SDR1 and SDR2 models are due to the dependence of models on $\widetilde{k}$ and $\widetilde{\varepsilon}$ and also due to the lack of flow history effects on the evolution of $\widetilde{\varepsilon}_c$. Furthermore for models relying on Σ transport

equation (SDR2 and FSD) a higher reaction rate can be predicted in these regions due to an infinite growth of term a in eq. (23) as it always produces Σ, which is not always the case as the flame induced turbulence scalar interaction can desroy the flame due to local changes in the alignment of the strain rate with respect to the flame gradients [53]. Both the FTI (algebraic) and FTI (transport equation) predict similar reaction rates in the immediate wake of the back ward facing step at $x/h = 1$ and $x/h = 3$ as shown in figures 8a and 8b. Further downstream at $x/h = 5$ and $x/h = 7$ the reaction rate prediction from the FTI (transport equation) model increases while the FTI (algebraic) model tends to predict a constant reaction rate as shown in figures 8c, 8d, 9d and 9e. An increase in the reaction rate in these regions is expected in the light of earlier results of Fureby [38] as regions of intense turbulence are bounded by the shear layer which widens as the distance from the step increases, thus leading to a much wider reaction zone. In order to quantify the difference between different models, percentage difference for the predicted peak reaction rate between the FTI (transport equation) and the other models is reported in table 3 for several locations downstream of the backward facing step.

A Schlieren photograph of the reacting flow from the experiment is presented in figure 9f. The brightest areas indicate the highest temperature gradients, which implies highest reaction rate regions. Figures 9a, 9b, 9c, 9d and 9e show the reaction rate predicted by FSD, SDR1, SDR2, FTI (algebraic) and FTI (transport equation) models respectively. In figure 9e, the predicted flame location given by the FTI transport equation is similar to that of the experiment, while the other models tend either to predict the reaction rate in the wrong location or under predict the reaction rate. This can be further validated by the comparison of Reynolds averaged progress variable from the simulations against the LES and experimental data as shown in figure 10. In this comparison the CO_2 mixture fraction is chosen as the progress variable from the experiment because it is identified as one of the deficient reactants as discussed by Cant et al [54]. The Reynolds average progress variable from the simulation is calculated as [55]:

$$\overline{c} = \widetilde{c} + \frac{\tau \widetilde{c''^2}}{1 + \tau \widetilde{c}}. \tag{24}$$

It can be noticed in figure 10 that the agreement between the predicted and the experimental values improves in case of FTI (transport equation) as the distance from the backward facing step increases. While the SDR1, SDR2 and FTI algebraic models yield similar results for the progress variable further downstream of the backward facing step at $x/h = 3.5$ and $x/h = 5.4$. The FSD model leads to slightly different results away from the backward facing step ($x/h = 3.5$ and $x/h = 5.4$) when compared with the other models, as it does not include the transport equation for $\widetilde{c''^2}$ and the variance of the progress variable takes the classical Bray Moss Libby (BML) form $\widetilde{c''^2} = \widetilde{c}(1 - \widetilde{c})$.

4.2.1 Overall assessment of models

In the light of the current calculations it is found that the numerical implementation for the FTI (transport equation) is the most difficult, when compared with other modelling approaches (FTI (algebraic), SDR1, SDR2 and FSD). The SDR1 model is the easiest to implement, where as SDR2, FSD and FTI (algebraic) models require several transport equations to close the models and are more difficult to implement. Generally the implementation of a model becomes difficult as the number of transport equations required to close the model increase. FTI (transport equation) requires closures for higher moments which are not easy to close when compared to the other models. Overall all the models tested in this study perform reasonably well for predicting the trends for mean velocities

and flame locations. The FTI (transport equation) does improve the results at some locations in the flow field when compared with other models in this study. More tests are needed to explore the predictive capabilities of the FTI modelling approach.

5. Summary and conclusions

In this study different models for flame turbulence interaction (FTI) have been compared. These include algebraic model for FTI proposed by Kolla et al [22](FTI algebraic model), FTI transport equation proposed by Ahmed et al [21](FTI transport model), the flame surface density (FSD) based approach and algebraic models for scalar dissipation $(\widetilde{\varepsilon}_c)$ proposed by Kolla et al [22](SDR1) and Vervisch et al [23](SDR2). The performance of these models is tested on a propane-air premixed flame with an equivalence ratio (ϕ) of 0.57 stabilised in a mixing layer. The results are compared with the experimental results of Pitz and Daily [24, 25] and Large Eddy Simulation (LES) results of Weller et al [37]. Initially isothermal simulations with the standard $k-\varepsilon$ and $k-\omega$ SST models are performed for the backward facing step configuration. It is found that both the turbulence models predict similar flow fields and the model performance is satisfactory for further modelling of the reacting flow.

The standard $k-\varepsilon$ model with wall functions is then used for testing flame turbulence interaction closures. It has been found that the SDR1, SDR2 and FSD models require a treatment for non-physical reaction rate prediction in the boundary layer regions near walls. Where as the models based on scalar dissipation transport equation do not require such treatments. This is due to the inclusion of the flow history effects of the scalar dissipation through its transport equation.

It is found that SDR1, SDR2 and FSD models yield similar results apart from the locations far downstream of the backward facing step. While the FTI (algebraic) and the FTI (transport equation) models predict similar results in the near wake region of the backward facing step. Further downstream all the models apart from the FTI (transport equation) deviate from the LES and experimental data. Better performance of the flame turbulence interaction transport equation in the downstream locations when compared with other modelling techniques is attributed to explicit inclusion of the strain rate and its flow history effects in the modelling strategy. Further tests for the flame turbulence interaction transport equation for higher Reynolds and a range of Karlovitz numbers are needed to confirm the model performance across a rage of combustion conditions. This forms part of the ongoing work.

Acknowledgements

The authors would like to thank the reviewers for their helpful and constructive comments regarding draft versions of this manuscript.

Appendix-A

Scalar dissipation transport equation

Terms on the right hand side of the scalar dissipation transport equation (eq. (7))

$$T_{11} = -\frac{\partial \overline{\rho u_i'' \varepsilon_c}}{\partial x_i}, \tag{25}$$

$$T_2 = 2\overline{\rho\varepsilon_c \frac{\partial u_l}{\partial x_l}}, \tag{26}$$

$$T_{32} = -2\overline{\rho\alpha}\left(\widetilde{\frac{\partial c''}{\partial x_i} S''_{ij} \frac{\partial c''}{\partial x_j}}\right), \tag{27}$$

$$T_4 = 2\left(\overline{\alpha \frac{\partial c''}{\partial x_j} \frac{\partial \dot{\omega}''_c}{\partial x_j}}\right), \tag{28}$$

$$D_2 = \overline{2\rho\left(\alpha \frac{\partial^2 c''}{\partial x_i \partial x_j}\right)^2}. \tag{29}$$

Flame turbulence interaction transport equation

Terms on the right hand side of the flame turbulence interaction transport equation (eq. (16))

$$D_f = -\overline{2\rho\alpha\alpha \frac{\partial}{\partial x_n}\left(\frac{\partial c''}{\partial x_j}\right)\frac{\partial}{\partial x_n}\left(\frac{\partial c''}{\partial x_i} S''_{ij}\right)} - \overline{2\rho\alpha\alpha \frac{\partial}{\partial x_n}\left(\frac{\partial c''}{\partial x_i}\frac{\partial c''}{\partial x_j}\frac{\partial}{\partial x_n} S''_{ij}\right)}$$
$$-\overline{2\rho\alpha\alpha \frac{\partial}{\partial x_n}\left(\frac{\partial c''}{\partial x_j} S''_{ij}\frac{\partial}{\partial x_n}\left(\frac{\partial c''}{\partial x_i}\right)\right)} + \overline{\alpha \frac{\partial c''}{\partial x_i}\frac{\partial c''}{\partial x_j}\frac{\partial}{\partial x_n}\left(\frac{\partial \tau''_{in}}{\partial x_j}\right)}. \tag{30}$$

$$F_1 = 2\overline{\alpha \frac{\partial c''}{\partial x_i} S''_{ij} \frac{\partial \dot{\omega}''_c}{\partial x_j}} - \overline{\alpha \frac{\partial c''}{\partial x_i}\frac{\partial c''}{\partial x_j}\frac{\partial}{\partial x_i}\left(\frac{\partial p'}{\partial x_j}\right)}. \tag{31}$$

$$F_D = 2\overline{\rho\alpha}\,\widetilde{\frac{\partial c''}{\partial x_i} S''_{ij} \frac{\partial c''}{\partial x_j}\frac{\partial u''_l}{\partial x_l}} - 2\overline{\rho\alpha}\,\widetilde{\frac{\partial c''}{\partial x_j}\frac{\partial u''_l}{\partial x_l}}\widetilde{\frac{\partial c''}{\partial x_i} S''_{ij}} + \overline{\alpha \frac{\partial \rho}{\partial x_j}\frac{\partial p'}{\partial x_i}\frac{\partial c''}{\partial x_j}\frac{\partial c''}{\partial x_i}\frac{1}{\rho}}$$
$$-\overline{\alpha \frac{\partial \rho}{\partial x_j}\frac{\partial \tau''_{in}}{\partial x_n}\frac{\partial c''}{\partial x_i}\frac{\partial c''}{\partial x_j}\frac{1}{\rho}}. \tag{32}$$

$$F_{TS} = \overline{\rho\alpha}\,\widetilde{\frac{\partial c''}{\partial x_i} S''_{ij}\frac{\partial c''}{\partial x_n}\frac{\partial u''_n}{\partial x_j}} + 2\overline{\rho\alpha}\,\widetilde{\frac{\partial c''}{\partial x_n}\frac{\partial u''_n}{\partial x_j}}\widetilde{\frac{\partial c''}{\partial x_i} S''_{ij}} - \overline{\rho\alpha}\,\widetilde{\frac{\partial c''}{\partial x_i}\frac{\partial c''}{\partial x_j}\frac{\partial u''_n}{\partial x_j}\frac{\partial u''_i}{\partial x_n}}$$
$$+\overline{\rho\alpha}\,\widetilde{\frac{\partial c''}{\partial x_i}\frac{\partial c''}{\partial x_j}}\widetilde{\frac{\partial u''_n}{\partial x_j}\frac{\partial u''_i}{\partial x_n}} \tag{33}$$

Appendix-B

The turbulent flow filed is simulated by using two turbulence models. Some details of the turbulence models are given below.

$k-\varepsilon$ model

The most common form of the model developed by Jones and Launder [43] is used here. The transport equations used in $k-\varepsilon$ model are :

$$\frac{\partial \overline{\rho}\widetilde{k}}{\partial t}+\frac{\partial \overline{\rho}\widetilde{u}_i\widetilde{k}}{\partial x_i}=\frac{\partial}{\partial x_j}\left[\left(\mu+\frac{\mu_t}{\sigma_k}\right)\frac{\partial \widetilde{k}}{\partial x_j}\right]+\overline{\rho}P_{k-\varepsilon}-\overline{\rho}\widetilde{\varepsilon}, \tag{34}$$

$$\frac{\partial \overline{\rho}\widetilde{\varepsilon}}{\partial t}+\frac{\partial \overline{\rho}\widetilde{u}_i\widetilde{\varepsilon}}{\partial x_i}=\frac{\partial}{\partial x_i}\left[\left(\mu+\frac{\mu_t}{\sigma_\varepsilon}\right)\frac{\partial \widetilde{\varepsilon}}{\partial x_i}\right]+C_{\varepsilon 1}\overline{\rho}\frac{\widetilde{\varepsilon}}{\widetilde{k}}P_{k-\varepsilon}-C_{\varepsilon 2}\overline{\rho}\frac{\widetilde{\varepsilon}^2}{\widetilde{k}}, \tag{35}$$

where

$$P_{k-\varepsilon}=-\overline{\rho}\widetilde{u_i''u_j''}\frac{\partial \widetilde{u}_i}{\partial x_j}. \tag{36}$$

The turbulent viscosity μ_t is calculated as :

$$\mu_t=C_\mu\overline{\rho}\frac{\widetilde{k}^2}{\widetilde{\varepsilon}} \tag{37}$$

The model constants $C_\mu, C_{\varepsilon 1}$ and $C_{\varepsilon 2}$ in eq.(34) and eq.(35)are given in table(4).

$k-\omega$ SST model

The standard $k-\omega$ SST model proposed by Menter [44] is also used for comparison. It blends the $k-\omega$ formulation in the boundary layer and the free stream independence of the $k-\varepsilon$ model in the far field. The governing equations for $k-\omega$ SST model are :

$$\frac{\partial \overline{\rho}\widetilde{k}}{\partial t}+\frac{\partial \overline{\rho}\widetilde{u}_i\widetilde{k}}{\partial x_j}=\frac{\partial}{\partial x_j}\left[\left(\mu+\frac{\mu_t}{\sigma_k}\right)\frac{\partial \widetilde{k}}{\partial x_j}\right]+P_{k-\omega}-\beta^*\overline{\rho}\widetilde{\omega}\widetilde{k}, \tag{38}$$

$$\begin{aligned}\frac{\partial \overline{\rho}\widetilde{\omega}}{\partial t}+\frac{\partial \overline{\rho}\widetilde{u}_j\widetilde{\omega}}{\partial x_j}=&\frac{\partial}{\partial x_j}\left[\left(\mu+\frac{\mu_t}{\sigma_\omega}\right)\frac{\partial \widetilde{\omega}}{\partial x_j}\right]+\overline{\rho}\gamma\left\|\overline{S}\right\|^2-\beta\overline{\rho}\widetilde{\omega}^2\\&+2\left(1-F_1\right)\frac{\overline{\rho}}{\sigma_{\omega_2}\widetilde{\omega}}\frac{\partial \widetilde{k}}{\partial x_j}\frac{\partial \widetilde{\omega}}{\partial x_j},\end{aligned} \tag{39}$$

where

$$P_{k-\omega}=min\left(-\overline{\rho}\widetilde{u_i''u_j''}\frac{\partial \widetilde{u}_i}{\partial x_j},10\beta^*\widetilde{k}\widetilde{\omega}\right). \tag{40}$$

Any coefficient α in this model is calculated from

$$\alpha = F_1 \alpha_1 + (1 - F_1)\, \alpha_2, \tag{41}$$

where subscript 1 corresponds to the coefficients in the $k-\omega$ model and subscript 2 corresponds to the coefficients in the $k-\varepsilon$ model. F_1 is the blending function in eq.(39) defined as:

$$F_1 = tanh\left(arg_1^4\right), \tag{42}$$

where

$$arg_1 = min\left[max\left(\frac{\sqrt{\widetilde{k}}}{\beta^* \widetilde{\omega} y}; \frac{500\nu}{y^2 \widetilde{\omega}}\right); \frac{4\widetilde{k}}{\sigma_{\omega_2} CD_{k\omega} y^2}\right] \tag{43}$$

$$CD_{k\omega} = max\left(2\overline{\rho}\frac{1}{\sigma_{\omega_2}\widetilde{\omega}}\frac{\partial k}{\partial x_j}\frac{\partial \widetilde{\omega}}{\partial x_j}, 10^{-20}\right). \tag{44}$$

y in eq.(44) represents the the distance to the nearest wall, and $CD_{k\omega}$ is the positive part of the cross diffusion term [44]. The eddy viscosity is calculated as [44]:

$$\mu_t = \frac{\overline{\rho}\widetilde{k} a_1}{max\left(a_1 \widetilde{\omega}; \|S\| F_2\right)} \tag{45}$$

where

$$\left\|\overline{S}\right\| = \sqrt{2 S_{ij} S_{ij}} \tag{46}$$

$$F_2 = tanh\left(arg_2^2\right) \tag{47}$$

$$arg_2^2 = max\left(\frac{2\sqrt{\widetilde{k}}}{\beta^* \widetilde{\omega} y}; \frac{500\nu}{y^2 \widetilde{\omega}}\right) \tag{48}$$

The model constants for the $k-\omega$ SST model are given in table 5.

References

[1] R. Lindstedt and E. Vaos, *Transported PDF modeling of high-Reynolds-number premixed turbulent flames*, Combustion and Flame 145 (2006), pp. 495–511.

[2] S.B. Pope, *PDF methods for turbulent reactive flows*, Progress in Energy and Combustion Science 11 (1985), pp. 119–192.

[3] A. Klimenko and R.W. Bilger, *Conditional moment closure for turbulent combustion*, Progress in Energy and Combustion Science 25 (1999), pp. 595–687.

[4] S. Amzin, N. Swaminathan, J.W. Rogerson, and J.H. Kent, *Conditional moment closure for turbulent premixed flames*, Combustion Science and Technology 184 (2012), pp. 1743–1767.

[5] S. Amzin and N. Swaminathan, *Computations of turbulent lean premixed combustion using conditional moment closure*, Combustion Theory and Modelling 17 (2013), pp. 1125–1153.

[6] A. Kronenburg and E. Mastorakos, *The Conditional Moment Closure Model*, in *Turbulent Combustion Modeling*, T. Mastorakos E.and Echekki, ed., Springer, 2011, pp. 63–90.

[7] D.B. Spalding, *Mixing and chemical reaction in steady confined turbulent flames*, Proceedings of the Combustion Institute Symposium (International) on Combustion 13 (1971), pp. 649–657.

[8] K.N.C. Bray and J.B. Moss, *A unified statistical model of the premixed turbulent flame*, Acta Astronautica 4 (1977), pp. 291–319.

[9] K.N.C. Bray and P.A. Libby, *Interaction effects in turbulent premixed flames*, Physics of Fluids 19 (1976), p. 1687.

[10] K. Bray, *Modelling methods, Laminar flamelets and the Bray Moss Libby model*, in *Turbulent Premixed Flames*, N. Swaminathan and K.N.C. Bray, eds., Cambridge University Press, 2011, pp. 42–60.

[11] K.N.C. Bray, P.A. Libby, and J.B. Moss, *Unified modeling approach for premixed turbulent combustion-Part I: General formulation*, Combustion and Flame 61 (1985), pp. 87–102.

[12] N. Peters, *Turbulent Combustion*, Cambridge University Press, 2000.

[13] D. Bradley, P. Gaskell, and X. Gu, *Application of a Reynolds stress, stretched flamelet, mathematical model to computations of turbulent burning velocities and comparison with experiments*, Combustion and Flame 96 (1994), pp. 221–248.

[14] H. Kolla and N. Swaminathan, *Strained flamelets for turbulent premixed flames, I: Formulation and planar flame results*, Combustion and Flame 157 (2010), pp. 943–954.

[15] R.S. Cant, S.B. Pope, and K.N.C. Bray, *Modelling of flamelet surface-to-volume ratio in turbulent premixed combustion*, Twenty-third Symposium (International) on Combustion 23 (1991), pp. 809–815.

[16] S.B. Pope, *The evolution of surfaces in turbulence*, International Journal of Engineering Science 26 (1988), pp. 445–469.

[17] K.N.C. Bray, *The interaction between turbulence and combustion*, Seventeenth Symposium Symposium (International) on Combustion 17 (1979), pp. 223–233.

[18] R. Borghi, *Turbulent premixed combustion: Further discussions on the scales of fluctuations*, Combustion and Flame 80 (1990), pp. 304–312.

[19] N. Chakraborty, M. Champion, A. Mura, and N. Swaminathan, *Modelling methods, Scalar dissipation rate approach*, in *Turbulent Premixed Flames*, N. Swaminathan and K.N.C. Bray, eds., Cambridge University Press, 2011, pp. 74–102.

[20] R.S. Cant and E. Mastorakos, *An introduction to turbulent reacting flows*, Imperial College Press, 2008.

[21] U. Ahmed, R. Prosser, and A.J. Revell, *Towards the development of an evolution equation for flame turbulence interaction in premixed turbulent combustion*, Flow, Turbulence and Combustion 93 (2014), pp. 637–663.

[22] H. Kolla, J.W. Rogerson, N. Chakraborty, and N. Swaminathan, *Scalar dissipation rate modeling and its validation*, Combustion Science and Technology 181 (2009), pp. 518–535.

[23] L. Vervisch, R. Hauguel, P. Domingo, and M. Rullaud, *Three facets of turbulent combustion modelling: DNS of premixed V-flame, LES of lifted nonpremixed flame and RANS of jet-flame*, Journal of Turbulence 5 (2004), pp. 37–41.

[24] R.W. Pitz and J.W. Daily, *An experimental study of combustion: The turbulent structure of a reacting shear layer formed at a rearward-facing step*, Tech. Rep., NASA, Lewis research center (contract number 165427), 1981.

[25] R.W. Pitz and J.W. Daily, *Combustion in a turbulent mixing layer formed at a rearward-facing step*, AIAA Journal 21 (1983), pp. 1565–1570.

[26] P.A. Libby and K.N.C. Bray, *Countergradient diffusion in premixed turbulent flames*, AIAA Journal 19 (1981), pp. 205–213.

[27] D. Veynante, A. Trouvé, K.N.C. Bray, and T. Mantel, *Gradient and counter-gradient scalar transport in turbulent premixed flames*, Journal of Fluid Mechanics 332 (1997), pp. 263–293.

[28] R. Cant, *RANS and LES modelling of premixed combustion*, in *Turbulent Combustion Modeling*, T. Mastorakos E.and Echekki, ed., Springer, 2011, pp. 63–90.

[29] M.M. Salehi and W.K. Bushe, *Presumed PDF modeling for RANS simulation of turbulent premixed flames*, Combustion Theory and Modelling 14 (2010), pp. 381–403.

[30] N. Swaminathan and K.N.C. Bray, *Effect of dilatation on scalar dissipation in turbulent premixed flames*, Combustion and Flame 143 (2005), pp. 549–565.

[31] N. Chakraborty, J.W. Rogerson, and N. Swaminathan, *A priori assessment of closures for scalar dissipation rate transport in turbulent premixed flames using direct numerical simulation*, Physics of Fluids 20 (2008), p. 045106.

[32] N. Chakraborty and N. Swaminathan, *Influence of the Damköhler number on turbulence-scalar interaction in premixed flames. II. Model development*, Physics of Fluids 19 (2007), p. 045104.

[33] N. Chakraborty and N. Swaminathan, *Reynolds number effects on scalar dissipation rate transport and*

its modeling in turbulent premixed combustion, Combustion Science and Technology 185 (2013), pp. 676–709.

[34] Y. Minamoto, N. Fukushima, M. Tanahashi, T. Miyauchi, T.D. Dunstan, and N. Swaminathan, *Effect of flow-geometry on turbulence-scalar interaction in premixed flames*, Physics of Fluids 23 (2011), p. 125107.

[35] T. Poinsot and D. Veynante, *Theoretical and Numerical Combustion*, 2nd ed., R.T.Edwards, Inc, 2005.

[36] R. Prasad, R. Paul, Y. Sivathanu, and J. Gore, *An evaluation of combined flame surface density and mixture fraction models for nonisenthalpic premixed turbulent flames*, Combustion and Flame 117 (1999), pp. 514–528.

[37] H. Weller, G. Tabor, A. Gosman, and C. Fureby, *Application of a flame-wrinkling LES combustion model to a turbulent mixing layer*, Symposium (International) on Combustion 27 (1998), pp. 899–907.

[38] C. Fureby, *Homogenization based LES for turbulent combustion*, Flow, Turbulence and Combustion 84 (2010), pp. 459–480.

[39] E. Tangermann, R. Keppeler, and M. Pfitzner, *Premixed turbulent combustion models for large eddy and RANS simulations*, in *ASME Turbo Expo 2010: Power for Land, Sea, and Air*, 2010, pp. 203–212.

[40] F. Archambeau, N. Mechitoua, and M. Sakiz, *A finite volume method for the computation of turbulent incompressible flows - industrial applications.*, Int. J. Finite Volumes 1 (2004), pp. 1–62.

[41] N. Jarrin, R. Prosser, J.C. Uribe, S. Benhamadouche, and D.R. Laurence, *Reconstruction of turbulent fluctuations for hybrid RANS/LES simulations using a Synthetic-Eddy Method*, International Journal of Heat and Fluid Flow 30 (2009), pp. 435–442.

[42] H.Q. Dong, V. Robin, A. Mura, and M. Champion, *Analysis of algebraic closures of the mean scalar dissipation rate of the progress variable applied to stagnating turbulent flames*, Flow, Turbulence and Combustion 90 (2012), pp. 301–323.

[43] W.P. Jones and B. Launder, *The prediction of laminarization with a two-equation model of turbulence*, Int.J. Heat Mass Transfer 15 (1972), pp. 301–314.

[44] F.R. Menter, *Two-equation eddy-viscosity turbulence models for engineering applications*, AIAA Journal 32 (1994), pp. 1598–1605.

[45] A.J. Revell, T.J. Craft, and D.R. Laurence, *Turbulence modelling of unsteady turbulent flows using the stress strain lag model*, Flow, Turbulence and Combustion 86 (2010), pp. 129–151.

[46] H.K. Versteeg and W. Malalasekera, *An Introduction to Computational Fluid Dynamics The Finite Volume Method*, 2nd ed., Pearson Education Limited, 2007.

[47] E. Furbo, *Evaluation of RANS turbulence models for flow problems with significant impact of boundary layers*, Master's thesis, Uppsala Universitet, 2010.

[48] T. Klein, T.J. Craft, and H. Iacovides, *Assessment of the performance of different classes of turbulence models in a wide range of non-equilibrium flows*, International Journal of Heat and Fluid Flow 51 (2015), pp. 229–256.

[49] T. Simon Crispin, *Burning velocity and the influence of flame stretch*, Ph.D. thesis, University of Leeds, 1991.

[50] C.M. Vagelopoulos, F.N. Egolfopoulos, and C.K. Law, *Further considerations on the determination of laminar flame speeds with the counterflow twin-flame technique*, Symposium (International) on Combustion 25 (1994), pp. 1341–1347.

[51] R. Blint, *The relationship of the laminar flame width to flame speed*, Combustion Science and Technology 49 (1986), pp. 79–92.

[52] C. Catlin and R. Lindstedt, *Premixed turbulent burning velocities derived from mixing controlled reaction models with cold front quenching*, Combustion and Flame 85 (1991), pp. 427–439.

[53] S. Ruan, N. Swaminathan, and Y. Mizobuchi, *Investigation of flame stretch in turbulent lifted jet flame*, Combustion Science and Technology 186 (2014), pp. 243–272.

[54] R.S. Cant, B. Rogg, and K.N.C. Bray, *On laminar flamelet modelling of the mean reaction rate in a premixed turbulent flame*, Combustion Science and Technology 69 (1990), pp. 53–61.

[55] H. Kolla and N. Swaminathan, *Strained flamelets for turbulent premixed flames II: Laboratory flame results*, Combustion and Flame 157 (2010), pp. 1274–1289.

C_a	C_b	C_c
$-4-\frac{1.9erf\left(Re_{l_t}\right)}{erf((Ka_L+1)/50)}$	$-3.5-\frac{0.01erf(Ka_L)}{0.01+\sqrt{erf\left(Re_{l_t}\right)}}$	$\frac{0.01+3.5erf(Ka_L)}{13erf\left(\left(Re_{l_t}^3/17.5\right)+0.01\right)}$

Table 1. Scaling factors for the flame turbulence interaction transport equation [21]

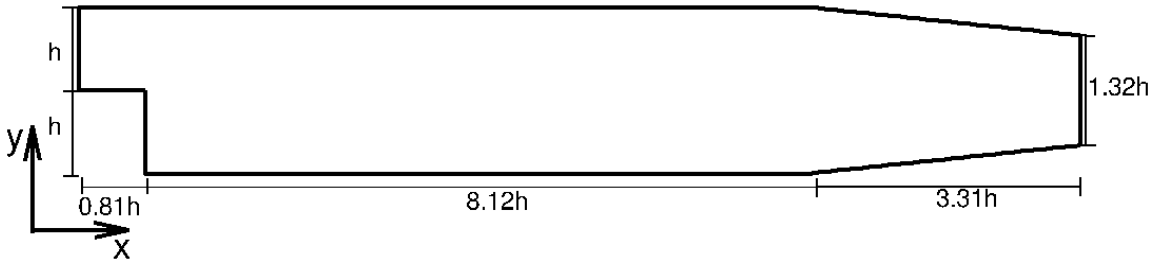

Figure 1. Schematic of the computational domain ($h = 0.0254m$)

$u_0(m/s)$	$p_0(atm)$	$T_0(K)$
13.3	1	293

Table 2. Inlet parameters for the simulation

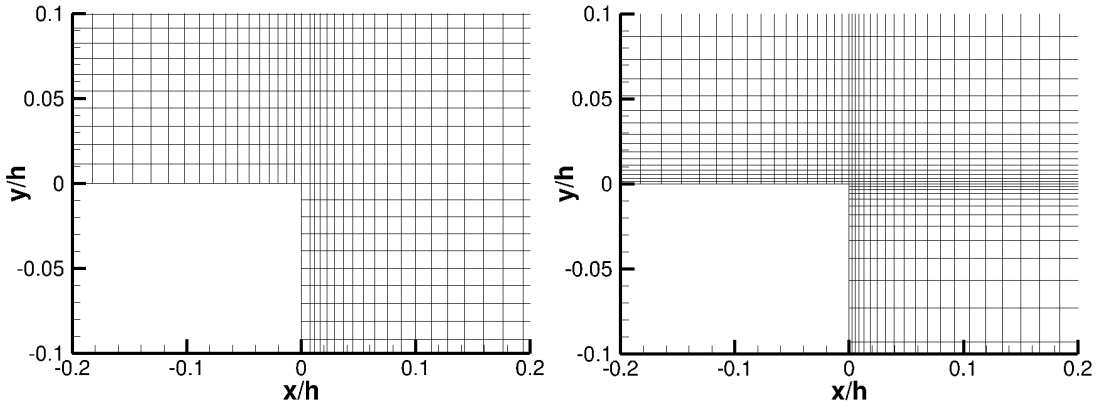

(a) Mesh near the backward facing step for $k-\varepsilon$ model, $y^+ \approx 30$ at the wall

(b) Mesh near the backward facing step $k-\omega$ SST model, $y^+ \approx 1$ at the wall

Figure 2. Meshs used for different turbulence models

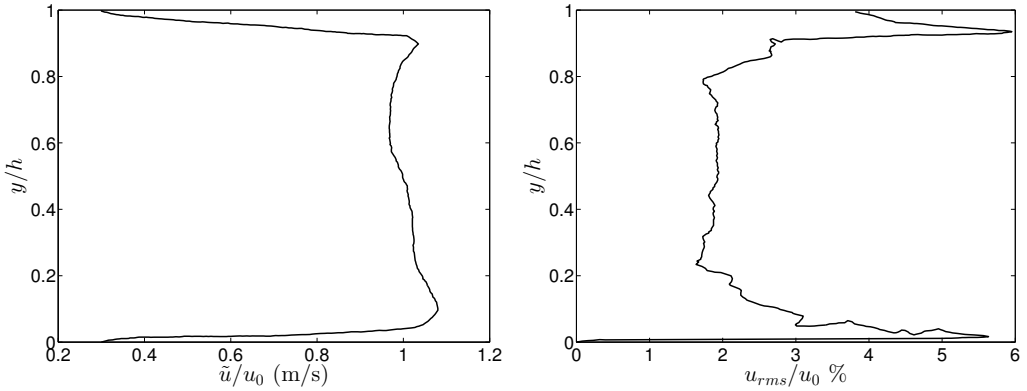

(a) Mean velocity profile at the inlet for isothermal simulations

(b) Turbulence intensity profile at the inlet for isothermal simulations

Figure 3. Inlet profiles for isothermal flow simulation [24]

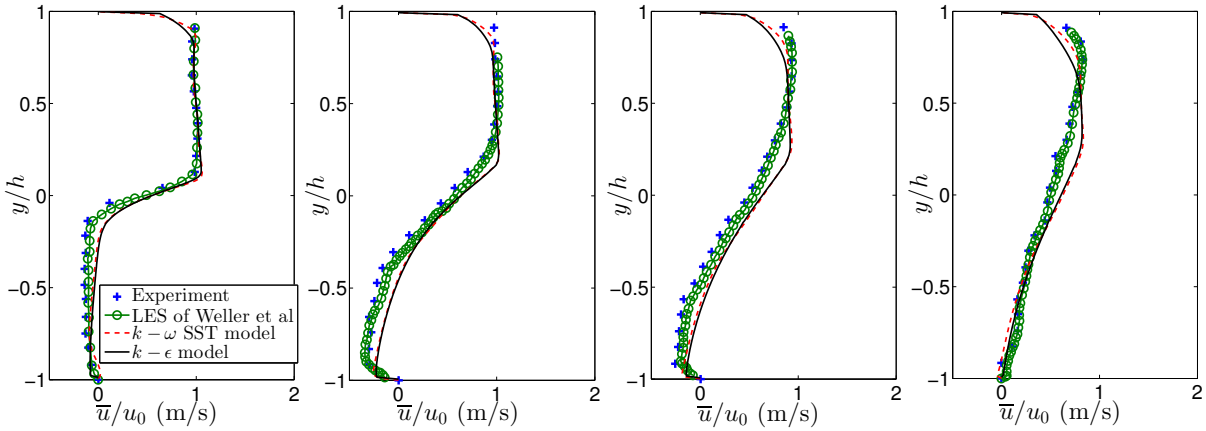

(a) $x/h = 1$ (b) $x/h = 3$ (c) $x/h = 5$ (d) $x/h = 7$

Figure 4. Isothermal flow velocity profiles

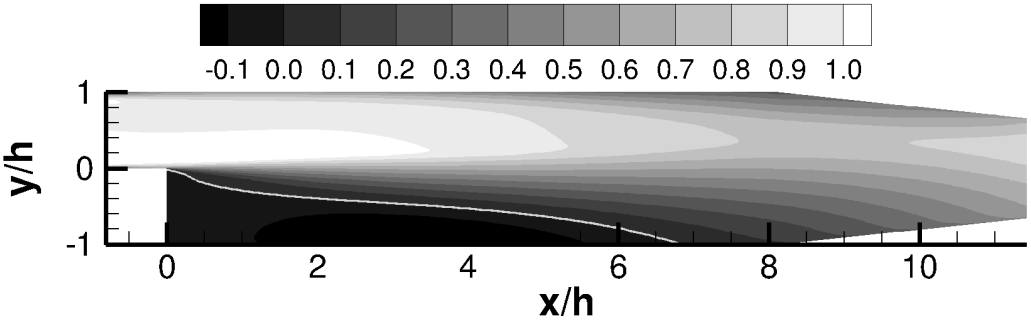

(a) Isothermal flow velocity $(\overline{u}/u_0)$ contours with $k-\varepsilon$ model. White line represents $\overline{u}/u_0 = 0$

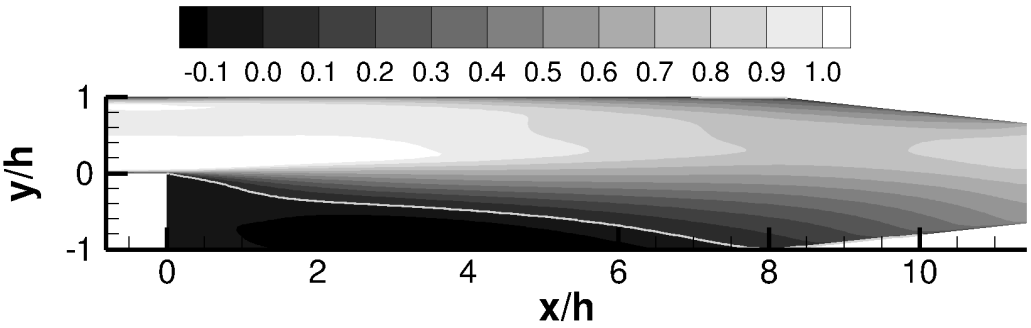

(b) Isothermal flow velocity $(\overline{u}/u_0)$ contours with $k-\omega$ SST model. White line represents $\overline{u}/u_0 = 0$

Figure 5. Isothermal flow velocity contours

x/h	SDR1	SDR2	FSD (transport equation)	FTI (algebraic)
1	−47%	−94.0%	−93.0%	0.7%
3	−15.7%	−40.0%	−45.0%	11.0%
5	2.9%	22.7%	−11.0%	25.0%
7	14.0%	79.0%	35.5%	39.0%

Table 3. Percentage difference for the maximum reaction rate prediction of FTI transport equation with different models

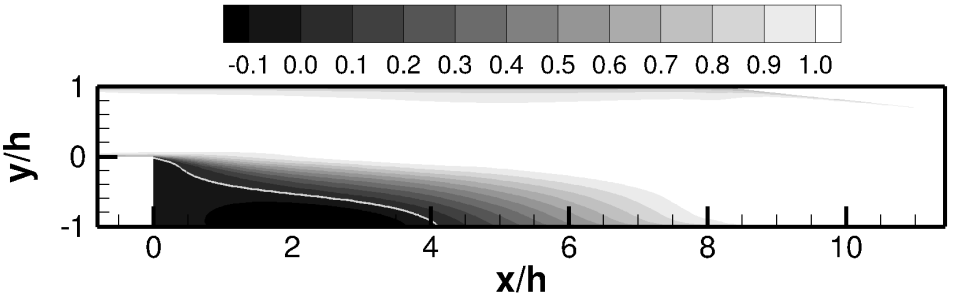

(a) FSD transport equation

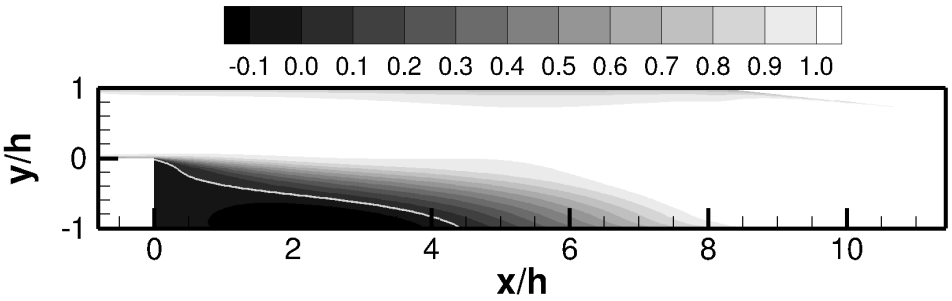

(b) Algebraic SDR 1

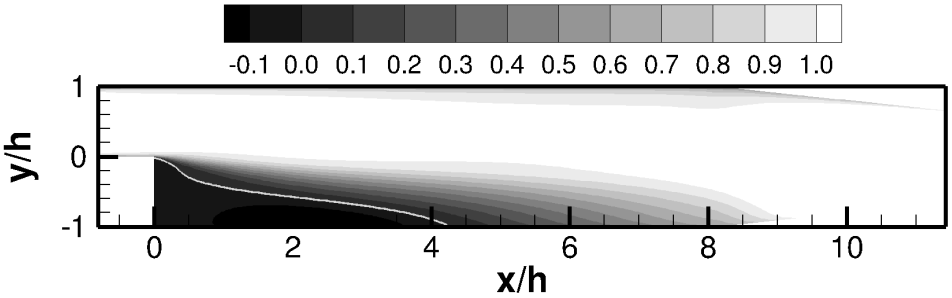

(c) Algebraic SDR 2

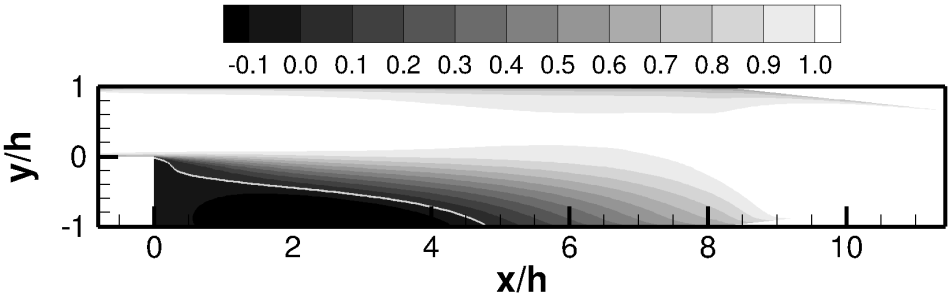

(d) FTI algebraic model

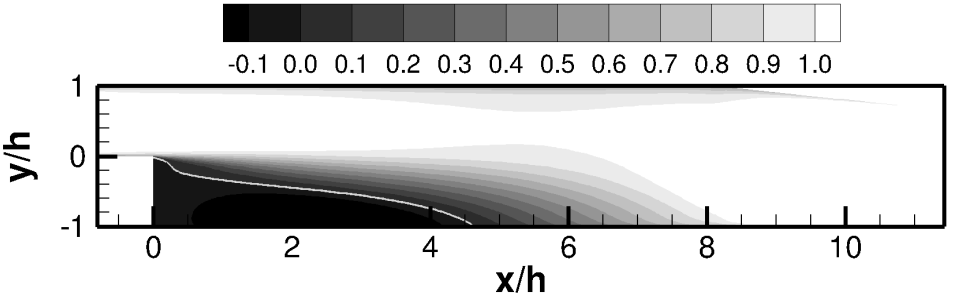

(e) FTI transport equation

Figure 6. Reacting flow velocity ($\widetilde{u}/u_o$) contours with $k-\varepsilon$ model. White lines represent $\widetilde{u}/u_0 = 0$.

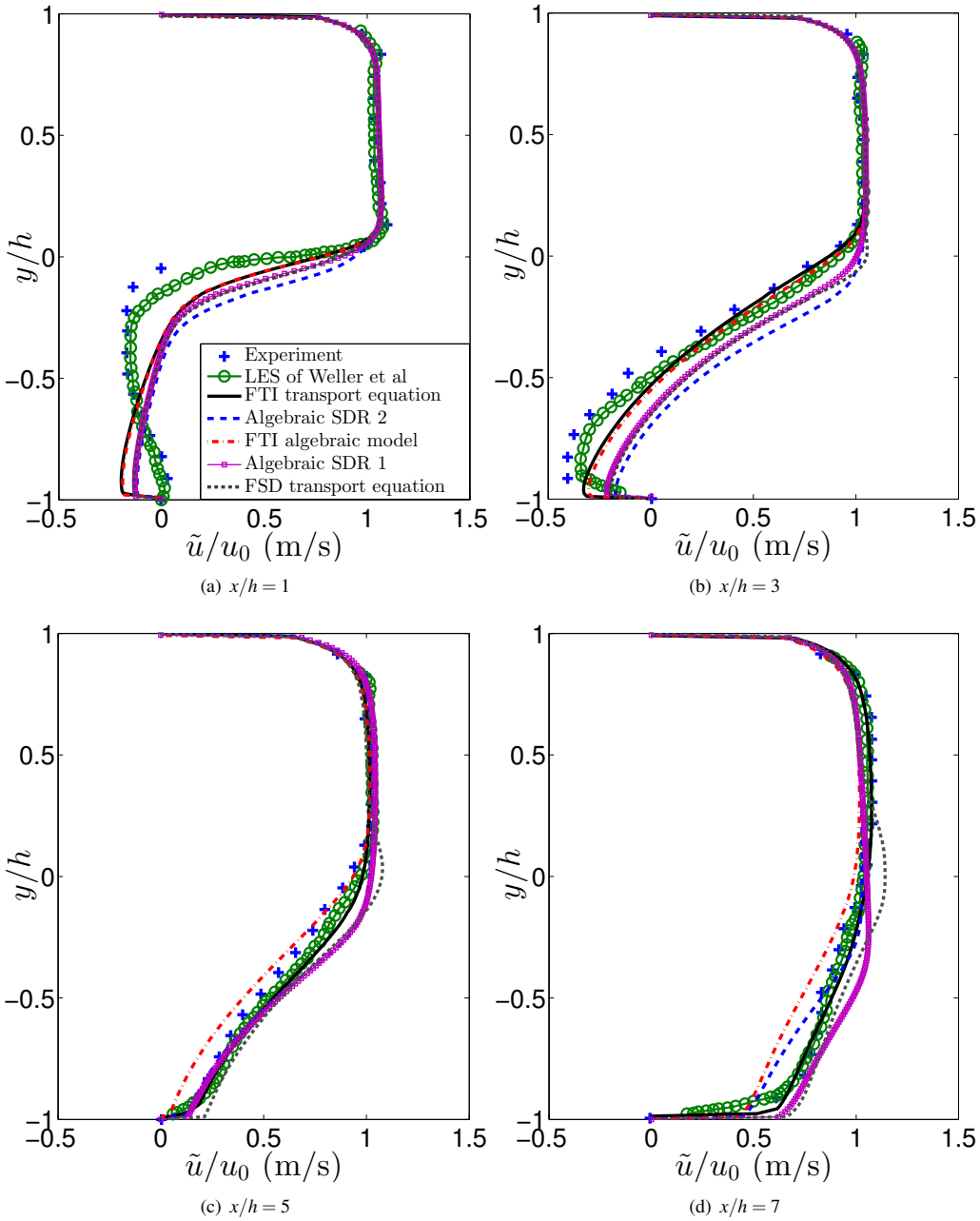

(a) $x/h = 1$ (b) $x/h = 3$

(c) $x/h = 5$ (d) $x/h = 7$

Figure 7. Reacting flow velocity profiles

C_μ	σ_k	σ_ε	$C_{\varepsilon 1}$	$C_{\varepsilon 2}$
0.09	1.0	1.3	1.44	1.92

Table 4. Values of the empirical constants in the $k-\varepsilon$ model

σ_{k_1}	σ_{ω_1}	β_1	a_1	β^*	κ	γ_1	σ_{k_2}	σ_{ω_2}	β_2	γ_2
1.176	2.0	0.075	0.31	0.09	0.41	$\frac{\beta_1}{\beta^*} - \frac{\kappa^2}{\sigma_{\omega 1}\sqrt{\beta^*}}$	1.0	1.168	0.0828	$\frac{\beta_2}{\beta^*} - \frac{\kappa^2}{\sigma_{\omega 2}\sqrt{\beta^*}}$

Table 5. Model constants for the $k-\omega$ SST model

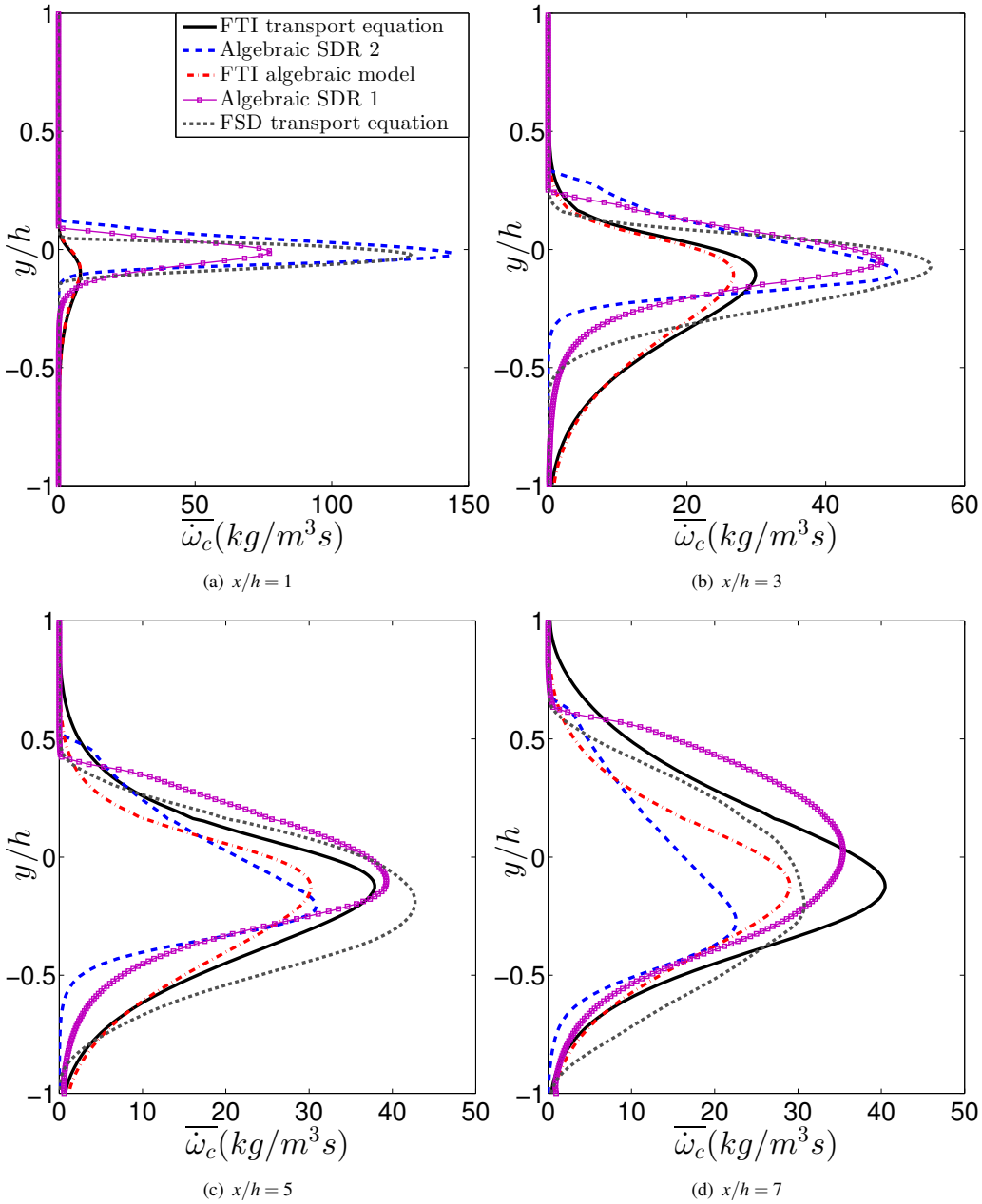

(a) $x/h = 1$ (b) $x/h = 3$

(c) $x/h = 5$ (d) $x/h = 7$

Figure 8. Reaction rate $\overline{\dot{\omega}}_c(kg/m^3s)$ profiles

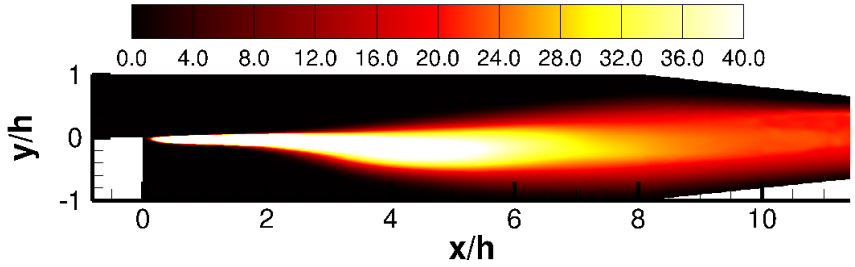

(a) reaction rate $\overline{\omega}_c(kg/m^3s)$ prediction by using FSD transport equation

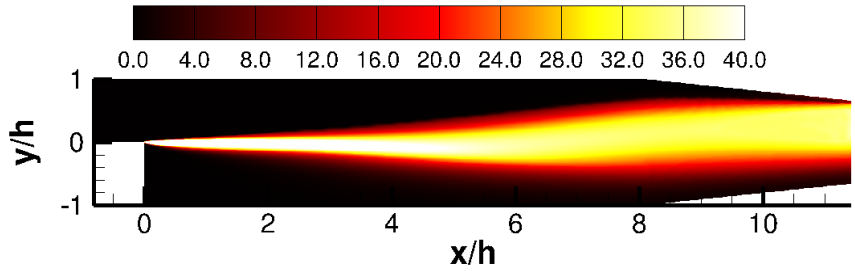

(b) reaction rate $\overline{\omega}_c(kg/m^3s)$ prediction by using algebraic SDR 1

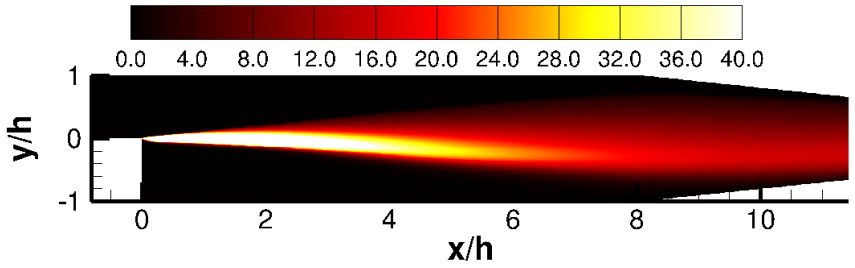

(c) reaction rate $\overline{\omega}_c(kg/m^3s)$ prediction by using algebraic SDR 2

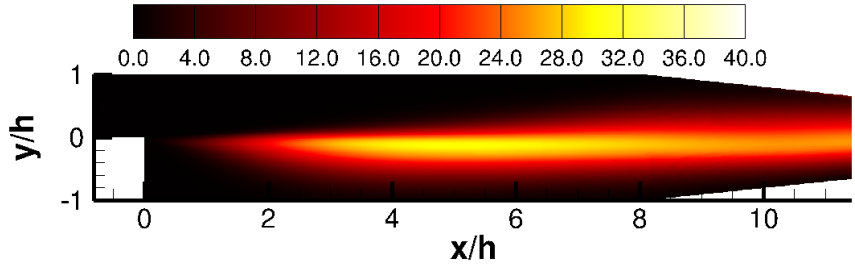

(d) reaction rate $\overline{\omega}_c(kg/m^3s)$ prediction by using FTI algebraic model

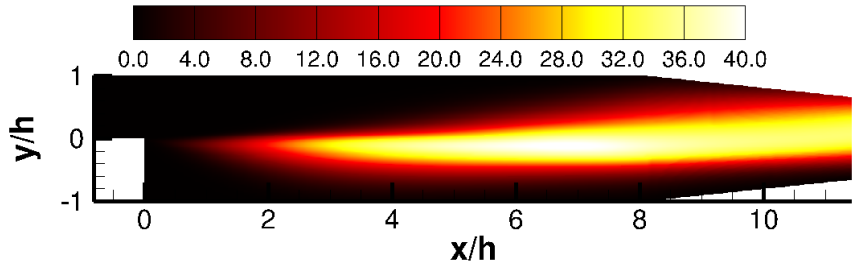

(e) reaction rate $\overline{\omega}_c(kg/m^3s)$ prediction by using FTI transport equation

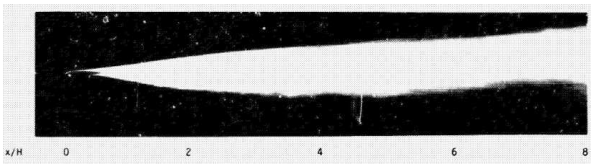

(f) Schileren photograph of the flame with an exposure time of 33*ms* (from [24])

Figure 9. Flame location and reaction rate in the domain

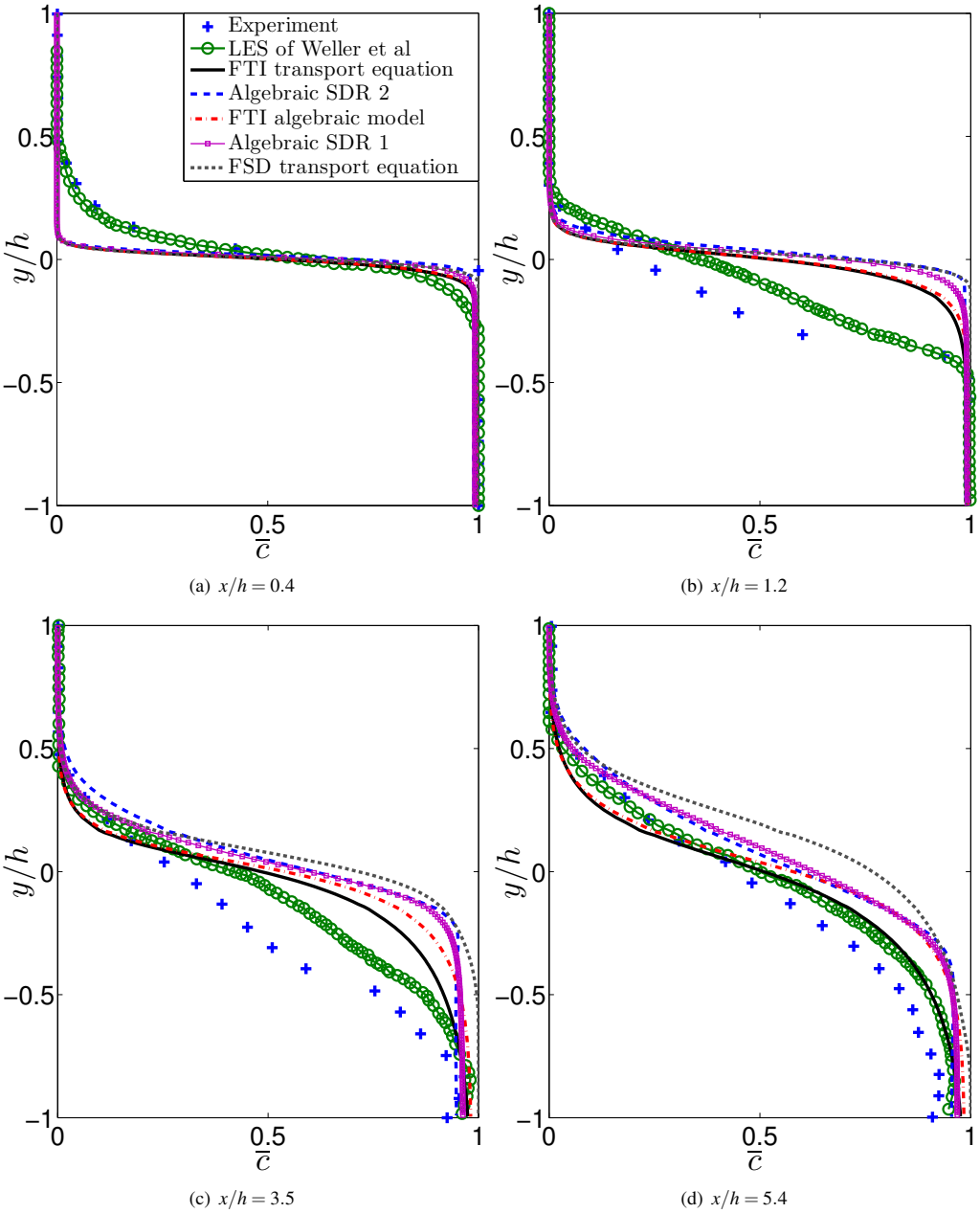

(a) $x/h = 0.4$ (b) $x/h = 1.2$

(c) $x/h = 3.5$ (d) $x/h = 5.4$

Figure 10. Reacting flow progress variable profiles